

# Differential connectivity and response dynamics of excitatory and inhibitory neurons in visual cortex

Sonja B Hofer<sup>1,6</sup>, Ho Ko<sup>1,6</sup>, Bruno Pichler<sup>1,5</sup>, Joshua Vogelstein<sup>2</sup>, Hana Ros<sup>1</sup>, Hongkui Zeng<sup>3</sup>, Ed Lein<sup>3</sup>, Nicholas A Lesica<sup>4</sup> & Thomas D Mrsic-Flogel<sup>1</sup>

Neuronal responses during sensory processing are influenced by both the organization of intracortical connections and the statistical features of sensory stimuli. How these intrinsic and extrinsic factors govern the activity of excitatory and inhibitory populations is unclear. Using two-photon calcium imaging *in vivo* and intracellular recordings *in vitro*, we investigated the dependencies between synaptic connectivity, feature selectivity and network activity in pyramidal cells and fast-spiking parvalbumin-expressing (PV) interneurons in mouse visual cortex. In pyramidal cell populations, patterns of neuronal correlations were largely stimulus-dependent, indicating that their responses were not strongly dominated by functionally biased recurrent connectivity. By contrast, visual stimulation only weakly modified co-activation patterns of fast-spiking PV cells, consistent with the observation that these broadly tuned interneurons received very dense and strong synaptic input from nearby pyramidal cells with diverse feature selectivities. Therefore, feedforward and recurrent network influences determine the activity of excitatory and inhibitory ensembles in fundamentally different ways.

The capacity of the neocortex to process sensory information depends on neuronal interactions between excitatory and inhibitory cell types. However, the relationships between the connectivity, receptive field properties and network dynamics of different cell types are not fully understood.

Most cortical neurons are sparsely interconnected excitatory pyramidal cells that typically show selective responses to different sensory features, and provide the main route of information flow to and from cortical areas. The remaining roughly 20% of cortical neurons consist of different subclasses of GABAergic inhibitory interneurons, which influence the firing and sensory responses of nearby pyramidal cells<sup>1–6</sup>.

In contrast to pyramidal cells, fast-spiking PV interneurons, which form the largest inhibitory subgroup<sup>1,2</sup>, form denser connections within local circuits<sup>7–9</sup>. The fraction of local excitatory inputs sampled by fast-spiking cells remains unclear, as reports vary from 19% (ref. 10) up to 60% (ref. 7) even in primary visual cortex (V1) of the same species (rat). The differences in connectivity between pyramidal cells and fast-spiking interneurons may influence the specificity with which these neuronal subpopulations respond to sensory stimuli, and the extent to which their co-activation is determined by sensory drive.

In V1, most layer 2/3 pyramidal cells respond selectively to oriented grating stimuli, possibly reflecting their nonrandom connectivity, whereby feedforward inputs from layer 4 and recurrent inputs from layer 2/3 are provided preferentially by neurons with similar response preferences<sup>11–15</sup>. On the other hand, there is considerable debate about the selectivity of visual responses and the functional

organization of connectivity of fast-spiking PV interneurons. In V1 of higher mammals, where neurons are arranged in functional columns, fast-spiking interneurons are often selective for orientation<sup>16–18</sup>. In mouse V1, where neurons with different orientation preferences are locally intermixed, fast-spiking PV cells and inhibitory neurons in general are reported to be more broadly tuned<sup>19–21</sup> (but see ref. 22). These findings suggest that fast-spiking interneurons receive non-selective excitatory input from the surrounding network<sup>23</sup>, and hence are more sharply tuned in species with orientation maps, but less well tuned in mice where neighboring pyramidal cells show diverse visual feature selectivity<sup>20</sup>. However, others find sharp orientation tuning of many fast-spiking PV interneurons in mouse V1 (ref. 22), suggesting that they receive input from subnetworks of pyramidal cells with similar orientation preferences<sup>10</sup>. Discerning between these apparently conflicting results is crucial for understanding the specificity with which these inhibitory neurons respond to sensory stimuli and influence the responses of other neurons in the network. It is therefore important to determine the response selectivity of a defined population of inhibitory neurons and any functional biases in their connectivity in the local circuit.

With differences in their local connectivity, populations of pyramidal cells and fast-spiking PV interneurons might also be expected to differ in their network interactions and in how their activity patterns are influenced by sensory stimuli. The organization of intracortical connections is thought to be reflected in patterns of spontaneous activity<sup>24</sup>. Some studies report similar patterns of spontaneous and evoked activity<sup>24–29</sup>, suggesting that intracortical connections influence activity patterns, such that a neuron is likely to fire with the

<sup>1</sup>Department of Neuroscience, Physiology and Pharmacology, University College London, London, UK. <sup>2</sup>Johns Hopkins University, Baltimore, Maryland, USA.

<sup>3</sup>Allen Institute for Brain Science, Seattle, Washington, USA. <sup>4</sup>Ear Institute, University College London, London, UK. <sup>5</sup>Present address: National Institute for Medical Research, Mill Hill, London, UK. <sup>6</sup>These authors contributed equally to this work. Correspondence should be addressed to T.D.M.-F. (t.mrsic-flogel@ucl.ac.uk).

Received 8 March; accepted 14 June; published online 17 July 2011; doi:10.1038/nn.2876

same interacting partners (ensemble) in the presence and absence of sensory input. By contrast, other studies find that even functionally similar neurons can fire independently of each other and that the strength of correlated firing in pairs of neurons can be influenced by sensory input<sup>30–35</sup>. At the level of local circuits, therefore, the degree to which sensory-evoked co-activations are influenced by intrinsic biases in connectivity, and how this relates to cell type, remains unresolved.

We have investigated the relationship between local synaptic connectivity, sensory response properties and the structure of network correlations in populations of pyramidal cells and fast-spiking PV interneurons in the same neuronal circuit. We applied two-photon calcium imaging<sup>36</sup> in layer 2/3 of mouse V1 to record spontaneous and visually evoked population activity with single-cell resolution<sup>37,38</sup> and to identify parvalbumin-expressing neurons genetically labeled with a red fluorescent protein<sup>39</sup>. We then used patch-clamp recordings in slices of the same tissue to determine local connectivity between a subset of neurons whose visual response properties were characterized *in vivo*. We found fundamental differences in both local synaptic connectivity and stimulus-dependence of neuronal co-activations in populations of pyramidal cells and fast-spiking PV interneurons, indicating that the influence between feedforward and recurrent drive differs across cortical cell types during the processing of visual information.

## RESULTS

### Visual responses of PV interneurons

We first measured the orientation tuning of genetically targeted, red fluorescent, PV cells, using parvalbumin-Cre (PV-Cre) mice crossed to a Cre-responsive reporter line (Ai9-*lsl*-tdTomato)<sup>39</sup>. Immunocytochemistry confirmed that red cells in layer 2/3 were almost exclusively parvalbumin-containing (92%, **Supplementary Fig. 1**). The electrophysiological properties of most red cells were typical of fast-spiking interneurons and none showed characteristics of excitatory pyramidal cells (**Supplementary Fig. 1**). We simultaneously imaged calcium signals and recorded action potential firing in PV cells by carrying out *in vivo* two-photon targeted loose-patch recordings of red cells in monocular V1 that was bulk labeled with injections of the calcium indicator dye OGB-1 AM (**Fig. 1a–e**). Confirming previous results<sup>20</sup>, changes in action potential firing were reflected in the calcium signal, even for neurons with high firing rates (**Fig. 1b–e** and **Supplementary Figs. 2–4**). For both putative pyramidal cells and fast-spiking PV cells the preferred orientation and the orientation selectivity (OSI) calculated from calcium signals were similar to values obtained from spiking responses (**Fig. 1f,g**). Calcium transient amplitude correlated well with the number of recorded action potentials for all cells (**Fig. 1d** and **Supplementary Fig. 2e**). The slope of this correlation varied between cells, partly depending on the maximum firing rate. When we plotted the size of the calcium transients against action potential number normalized to the maximum firing rate (for the range of gratings presented), we found a relatively similar (and nearly linear) relationship for all PV cells (**Fig. 1e**). There was also a clear correspondence between recorded action potentials and firing rate inferred from the calcium signal using a fast, non-negative deconvolution method<sup>40</sup> (see Online Methods) for both putative pyramidal cells (**Supplementary Fig. 2**) and PV neurons (**Supplementary Fig. 4**).

Having thus established that the calcium signal is a good indicator for changes in firing rate for neurons with very different firing frequencies, we used two-photon imaging to measure orientation selectivity for significantly responsive (see Online Methods) populations of

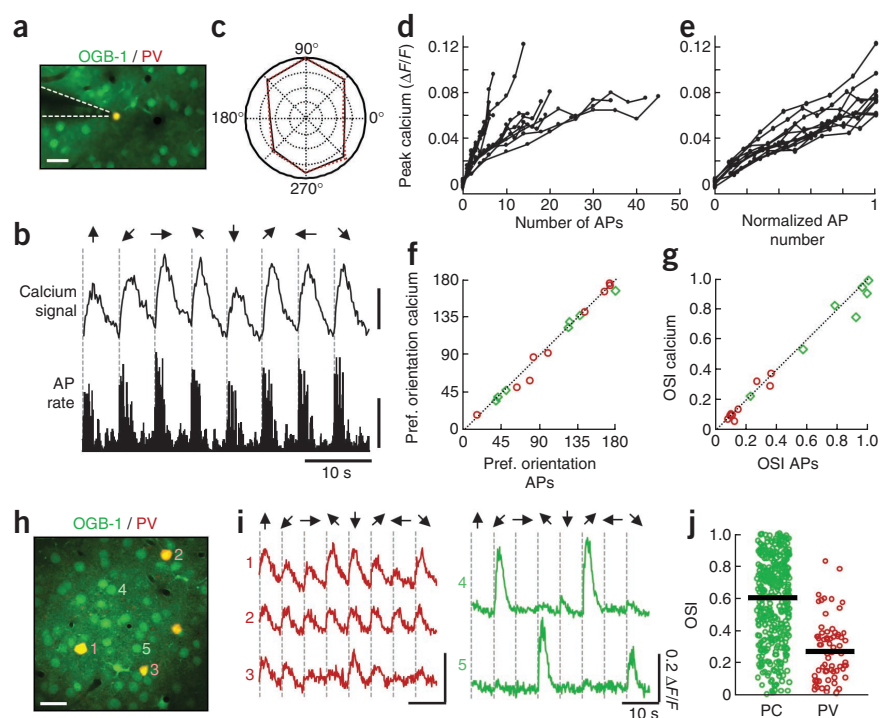
PV neurons and neurons not expressing the red protein (**Fig. 1h–j**), which primarily ( $\geq 90\%$ ) represent excitatory pyramidal cells<sup>2</sup>, and will therefore be referred to as pyramidal cells hereafter. As expected, most pyramidal cells responded selectively to oriented gratings and, on average, showed high orientation selectivity<sup>41</sup> (median OSI, 0.60; **Fig. 1i,j**). As a population, PV neurons responded much less selectively to moving gratings, as most showed broader orientation tuning (median OSI, 0.26; **Fig. 1i,j**), as was also apparent from the cell-attached recordings (median OSI<sub>spiking</sub>, 0.13; **Fig. 1g**). However, many PV neurons did show some orientation preference, including a smaller fraction more selective for orientation (OSI > 0.4 in 13/71 or 18% of significantly responsive PV neurons; **Fig. 1i,j**).

### Cell type-specific differences in synaptic connectivity

In layer 2/3 of rodent V1, pyramidal cells connect to each other sparsely<sup>7,11,12,23</sup> whereas fast-spiking interneurons, which typically express parvalbumin and constitute up to 10% of the cortical neuronal population<sup>2</sup>, are more densely connected to the surrounding network<sup>7–9,23</sup>. Pyramidal cells might form selectively interconnected subnetworks consisting of neurons with similar visual feature selectivity<sup>12</sup>, whereas fast-spiking interneurons might receive functionally unbiased input from surrounding pyramidal neurons and are hence more broadly tuned<sup>20,23</sup>. To test these hypotheses directly, we developed an approach to map synaptic connectivity between nearby neurons (<50  $\mu\text{m}$  apart) whose visual response properties had been functionally characterized *in vivo*<sup>11</sup>. We identified the same neurons in slices that had been imaged *in vivo*, and therefore were able to directly relate the connectivity of different neurons to their orientation tuning (**Fig. 2** and see Online Methods). By carrying out patch-clamp recordings from up to four neurons simultaneously, we assessed connectivity by stimulating one neuron at a time and observing postsynaptic potentials in each of the other neurons in turn. The presence or absence of short-latency postsynaptic potentials enabled us to determine the incidence and strength of synaptic connections. With this approach, we tested the dependency of connection probability on orientation tuning of pyramidal cells and fast-spiking interneurons.

As shown previously, connections between pyramidal cells in layer 2/3 of mouse V1 were weak and sparse (19%, 45 connections out of 235 tested; **Fig. 2d,e**), and preferentially but not exclusively formed between neurons with smaller differences in preferred orientations<sup>11</sup> ( $\Delta\text{Ori}$ ; **Fig. 2h**). By contrast, fast-spiking PV interneurons received input from neighboring pyramidal cells with remarkably high probability (88%, 36 of 41 tested, data from wild-type and PV-Cre-*lsl*-tdTomato mice, see Online Methods; **Fig. 2d**). We examined the orientation tuning curves for 17 fast-spiking cells together with the tuning profiles of pyramidal cells that responded to moving gratings and from which they received excitatory connections (**Fig. 2a,f,g**). Fast-spiking PV interneurons showed weak biases toward orientation (OSI range, 0.11–0.51; median, 0.22), and received inputs from both sharply and more broadly tuned pyramidal cells (OSI range, 0.07–1.00; median, 0.68) preferring a wide range of orientations or directions (**Fig. 2a,f,g**). As previously shown, among orientation-selective pyramidal cells (OSI > 0.4), the connectivity rate decreased monotonically with increasing difference in  $\Delta\text{Ori}$ <sup>11</sup> ( $P = 0.04$ , Cochran-Armitage test for trend; **Fig. 2h**). By contrast, we found no trend for the probability of connections between pyramidal cells and fast-spiking PV interneurons ( $P = 0.53$ , Cochran-Armitage test), because almost all pyramidal cells provided input to neighboring fast-spiking PV interneurons irrespective of how similarly they responded to visual stimulation or how selectively they responded

**Figure 1** Calcium imaging and electrophysiological recordings of visually evoked responses in PV neurons. **(a)** An OGB-1-labeled PV neuron in a Cre-PV-*Isl1*-tdTomato mouse from which a cell-attached recording was made. Scale bar, 20  $\mu\text{m}$ . **(b)** Average calcium signal ( $\Delta F/F$ , top) and action potential (AP) rate per imaging frame (bottom) from simultaneous calcium imaging and electrophysiological recording from a PV neuron during stimulation with drifting gratings. Scale bars, 5%  $\Delta F/F$ , 4 spikes per bin; bin size 131 ms. Directions of drifting gratings are shown; dashed lines show drift onset. **(c)** Polar plot of normalized responses to grating directions from neuron in **b**, calculated from action potentials (black solid line) and calcium signal (red dotted line). **(d,e)** Average peak calcium signal plotted against absolute number of action potentials (**d**) or number of action potentials normalized to maximum number of action potentials (**e**) for each of 12 PV neurons from 6 mice, calculated for bins of 393 ms. Error bars are omitted for clarity. **(f,g)** Correspondence of preferred grating orientation (**f**) and orientation selectivity index (OSI, see Online Methods; **g**) calculated from calcium signal and from action potentials for nine PV neurons (red circles) and seven pyramidal cells (green diamonds) that were visually stimulated and responsive to moving gratings. **(h)** OGB-1-labeled tissue, including four PV neurons (red) in layer 2/3. Scale bar, 20  $\mu\text{m}$ . **(i)** Average calcium traces ( $\Delta F/F$ ) from three PV neurons (red, left) and two parvalbumin-negative neurons (putative pyramidal cells, green, right) during stimulation with episodically presented drifting gratings (eight directions, six repetitions). The directions of drifting gratings are shown; dashed lines show drift onset. **(j)** OSI for pyramidal cells (green) and PV interneurons (red) that responded significantly to grating stimuli (ANOVA,  $P < 0.0001$ ). OSI for highly selective, sharply tuned neurons approaches 1, whereas OSI for broadly tuned, nonselective neurons approaches zero. Black lines, median OSI. Pyramidal cell: median OSI, 0.60; PV cells: median OSI, 0.26; 15 regions, 7 animals,  $P < 10^{-6}$ .



to grating orientation (**Fig. 2h**). Moreover, the strength of most connections between pyramidal cells and fast-spiking PV interneurons was an order of magnitude higher than that of connections between pairs of pyramidal cells (median excitatory postsynaptic potential (EPSP) amplitude of pyramidal cell–interneuron connection, 1.36 mV versus 0.20 mV for pyramidal cell–connections;  $P < 10^{-8}$ , rank sum test; **Fig. 2e**), a finding consistent with previous results in rat V1 (ref. 7). We also tested whether the strength of connections from pyramidal cells to fast-spiking PV cells or their short-term plasticity (paired-pulse-ratio, PPR) depended on the similarity of orientation tuning between two neurons (**Fig. 2i,j**), but found no significant trends ( $P > 0.1$ ).

These results indicate that fast-spiking cells receive very dense and strong input from nearby pyramidal neurons with diverse selectivities and preferences for stimulus orientation, and that this connectivity probably contributes to the broader tuning of fast-spiking interneurons.

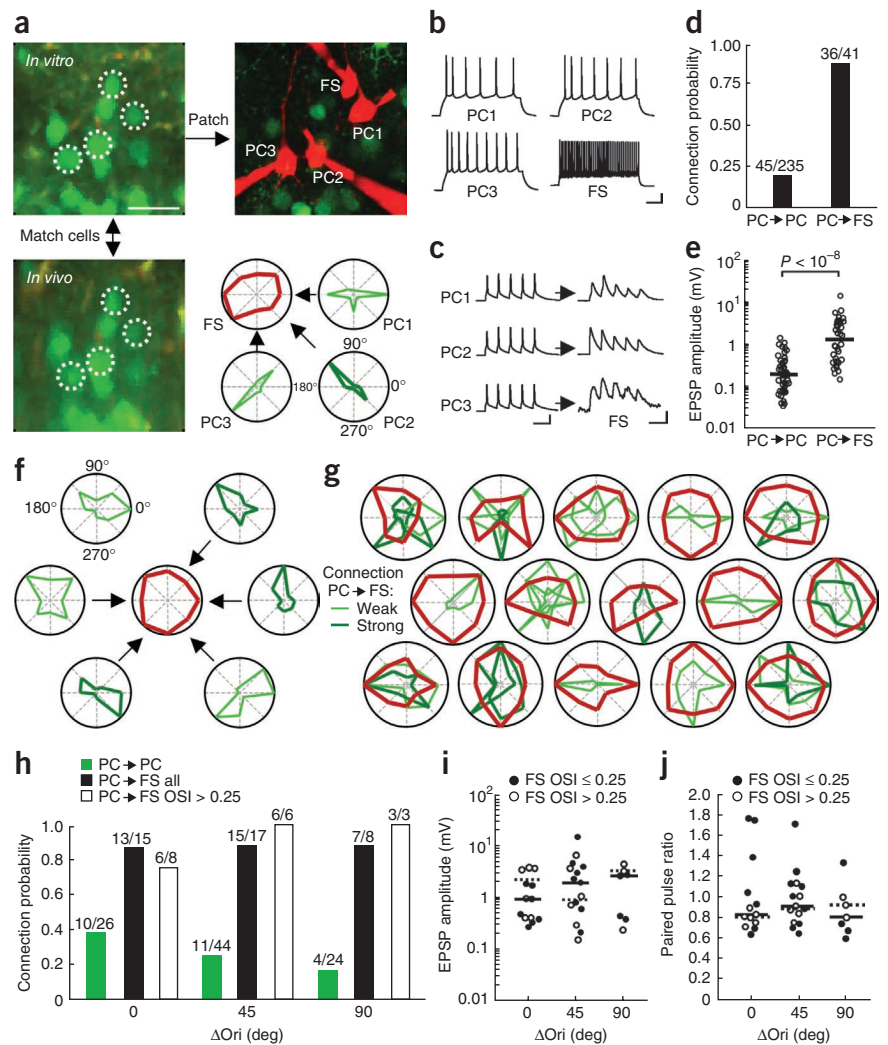
### Relationship between spontaneous and evoked activity

We next investigated the extent to which the differential connectivity profiles of pyramidal cells and fast-spiking PV cells might influence the activity dynamics of these two neuronal populations. We recorded spontaneous calcium signals in the dark in layer 2/3 of V1 in PV-Cre-*Isl1*-tdTomato mice and computed correlations of time-varying calcium signals for each neuronal pair over the duration of each recording (spontaneous correlation). Pair-wise correlations provided an indication of which neurons were likely to be spontaneously co-active. Given that spontaneous activity patterns have been suggested to reflect underlying connectivity in the network<sup>24,25</sup>, we expected the relationship between

spontaneous correlations and visual response similarity to resemble the relationship we had observed between visual response similarity and synaptic connectivity<sup>11</sup> (**Fig. 2**). To test this, we plotted the correlation strength of neuronal pairs during spontaneous activity against signal correlation (correlation of average responses, see Online Methods), which provides a measure of the similarity of neuronal responses to drifting gratings. We quantified the relationship between spontaneous correlation and signal correlation for pairs of pyramidal cells, pairs of PV cells and pairs consisting of one pyramidal cell and one PV cell, by computing the correlation ( $R$ ) and the slope of the linear fit (**Fig. 3a–c**). To visualize data from all animals in a single plot, we also normalized the pair-wise correlation values by calculating z-scores separately for each region (**Fig. 3d**; see Online Methods), because the average correlation strength varied between regions and animals (see also **Fig. 4**) and pooling the raw data together could introduce additional dependencies. We found only a very weak relationship between spontaneous and signal correlation for pyramidal cell pairs (median  $R = 0.18$ , median slope = 0.04; pooled data:  $R = 0.10$ ;  $P < 10^{-4}$ ; **Fig. 3**); pyramidal cells with similar responses to drifting gratings were only slightly more likely to fire together spontaneously than neurons with very different visual responses, and the scatter of data points was very large. There was a stronger relationship for pairs consisting of one pyramidal cell and one PV cell (median  $R = 0.33$ , median slope = 0.14; pooled data:  $R = 0.22$ ,  $P < 10^{-4}$ ; **Fig. 3**). In contrast to pyramidal cells, there was a strong relationship between signal and spontaneous correlation for pairs of PV cells, whereby cells that responded more similarly to gratings were more correlated during spontaneous activity, whereas those that responded less similarly were less correlated during spontaneous activity (median  $R = 0.68$ , median slope = 0.49; pooled data:  $R = 0.61$ ,  $P < 10^{-4}$ ; **Fig. 3**).

**Figure 2** Assessing synaptic connectivity *in vitro* between neurons functionally characterized *in vivo*.

(a) OGB-1-labeled V1 tissue in a slice (top left) and of the same cells *in vivo* before slicing (bottom left, after registration of the image stacks; see Online Methods). White circles, matched neurons *in vivo* and *in vitro*, which were targeted for whole-cell recording and filled with Alexa 594 (top right). Three pyramidal cells (PC1–3) and one fast-spiking interneuron (FS) were patched. Bottom right, polar plots of normalized responses to gratings drifting in eight directions, illustrating orientation/direction preference and tuning. Scale bar represents 30  $\mu\text{m}$ . (b) Action potential firing pattern in response to depolarizing current injection for cells from a. Scale bars: 20 mV, 50 ms. (c) Average traces of postsynaptic potentials in the fast-spiking interneuron in response to spike-evoking current injections in each of the three pyramidal cells (PCs) from a, showing that all three provided synaptic input onto the fast-spiking neuron. Scale bars: left, 40 mV, 50 ms; right, 2 mV (upper two), 0.2 mV (lower), 50 ms. (d) Probability of finding synaptic connections between pairs of pyramidal cells and from pyramidal cell to fast-spiking PV neurons. (e) Amplitudes of EPSPs between pyramidal cells and from pyramidal cells to fast-spiking PV cells. Black lines depict median amplitudes. (f) Another example of connectivity between six pyramidal cells and one fast-spiking PV interneuron and their orientation preferences. Five out of the six pyramidal cells provided input onto the fast-spiking PV neuron, which was held in whole-cell mode continuously while two sets of three pyramidal cells were patched and their connectivity assayed sequentially. (g) Polar plots with normalized responses to drifting grating stimuli (8 directions) of 15 more visually responsive, fast-spiking PV interneurons (red lines) overplotted with normalized responses of the pyramidal cells that provided synaptic input onto them (green lines). Pyramidal cells that provided stronger connections ( $>2$  mV EPSP amplitude) are indicated by darker and thicker green lines. (h) Relationship between connection probability and difference in preferred orientation ( $\Delta\text{Ori}$ ) for pairs of orientation-tuned (OSI  $> 0.4$ ) pyramidal cells (green), from pyramidal cells to fast-spiking PV interneurons (black) and from pyramidal cells to fast-spiking PV interneurons with OSI  $> 0.25$  (open bars). Two pyramidal cells were more likely to be connected if they preferred similar grating orientations. Connection probability from pyramidal cell onto fast-spiking PV cells did not depend on response similarity, irrespective of response selectivity. (i) Connection strength (EPSP amplitude) from pyramidal cells to fast-spiking PV cells plotted against  $\Delta\text{Ori}$ . Closed circles, pairs with OSI  $\leq 0.25$ ; open circles, pairs with OSI  $> 0.25$ . Strength of input did not depend on orientation preference similarity: all cell pairs,  $P = 0.59$ , only cell pairs with OSI  $> 0.25$ ,  $P = 0.94$ , Kruskal-Wallis test. (j) Relationship between paired-pulse ratio (PPR) of synaptic connections from pyramidal cells to fast-spiking PV cells and  $\Delta\text{Ori}$ . Degree of facilitation (PPR  $> 1$ ) or depression (PPR  $< 1$ ) of synapses was not related to response similarity to gratings: all cell pairs,  $P = 0.54$ , only cell pairs with OSI  $> 0.25$ ,  $P = 0.11$ , Kruskal-Wallis test. Black lines, median amplitudes; dotted lines, median amplitudes for pairs with OSI  $> 0.25$ . Bins include difference in preferred orientation values of 0–22.5° (0° bin), 22.5–67.5° (45° bin) and 67.5–90° (90° bin).



These results could be influenced by a documented relationship between correlation strength and cortical distance<sup>30</sup>. We also found a negative relationship between the strength of correlation of the activity of cell pairs with and without visual stimulation and cell distance. This negative relationship was stronger and 2–3-fold steeper for pairs of PV cells than for pairs of pyramidal cells (spontaneous activity: PV interneurons,  $R = -0.32$ , slope =  $-0.009$ ; pyramidal cells,  $R = -0.12$ , slope =  $-0.003$ ; **Supplementary Fig. 5a–c**). However, restricting our dataset to cell pairs less than 50  $\mu\text{m}$  apart did not alter the relationship between response similarity and spontaneous correlations (**Supplementary Fig. 5d–f**, compare with **Fig. 3d**), ruling out the idea that it was mostly brought about by distance effects.

The weak relationship between spontaneous correlation and visual response similarity in populations of pyramidal cells suggests that biased local connectivity among these neurons (**Fig. 2**) does not have a strong effect on the pattern of network co-activations. By contrast, there was a strong relationship between spontaneous correlation and visual response similarity in PV cells, suggesting that very dense and strong excitatory input from the local network strongly influences their activity during visual stimulation.

#### Structure of PV cell correlations is less stimulus dependent

The results from the previous section suggest that PV cells are influenced more than pyramidal cells by local network connectivity. To investigate the importance of this difference for visual processing,

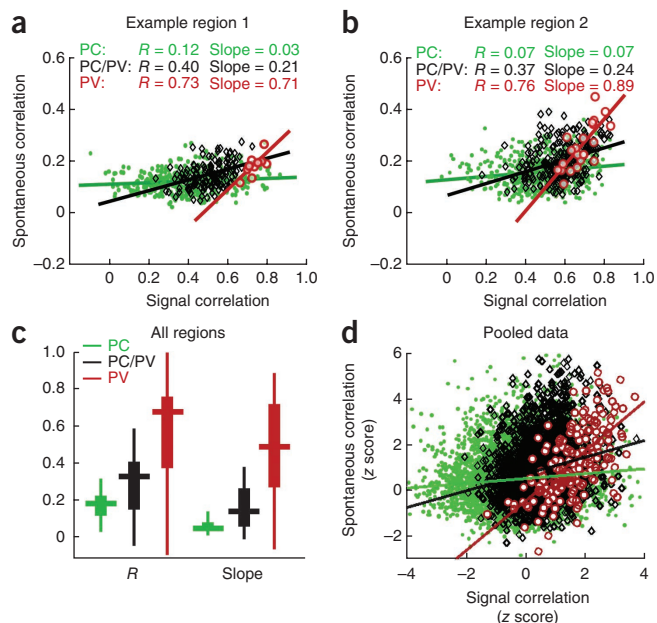


**Figure 3** Relationship between response similarity and pair-wise correlations during spontaneous activity. **(a,b)** Spontaneous pair-wise correlation coefficients plotted against pair-wise signal correlation coefficients (from averaged responses to gratings drifting in eight directions) from two imaging regions, for pairs of parvalbumin-negative neurons (pyramidal cells, PCs green), mixed pairs of one pyramidal cell and one PV neuron (black) and pairs of PV neurons (red). **(c)** Boxplots of the correlation coefficients ( $R$ ) and slopes of the relationship between spontaneous correlations and signal correlations from all imaged regions. Insert, horizontal lines are group medians. **(d)** Pooled data from all pyramidal cell pairs (green), mixed pairs (black) and PV cell pairs (red) normalized for comparison across animals and imaged regions by computing z-scores (see Online Methods). Pyramidal cell pairs:  $R = 0.10$ , slope = 0.11; pyramidal cell–PV cell pairs:  $R = 0.22$ , slope = 0.37; PV cell pairs:  $R = 0.61$ , slope = 1.08 (15 regions, 7 animals, 7,285 pyramidal cell pairs, 2,562 pyramidal cell–PV cell pairs, 187 PV cell pairs).

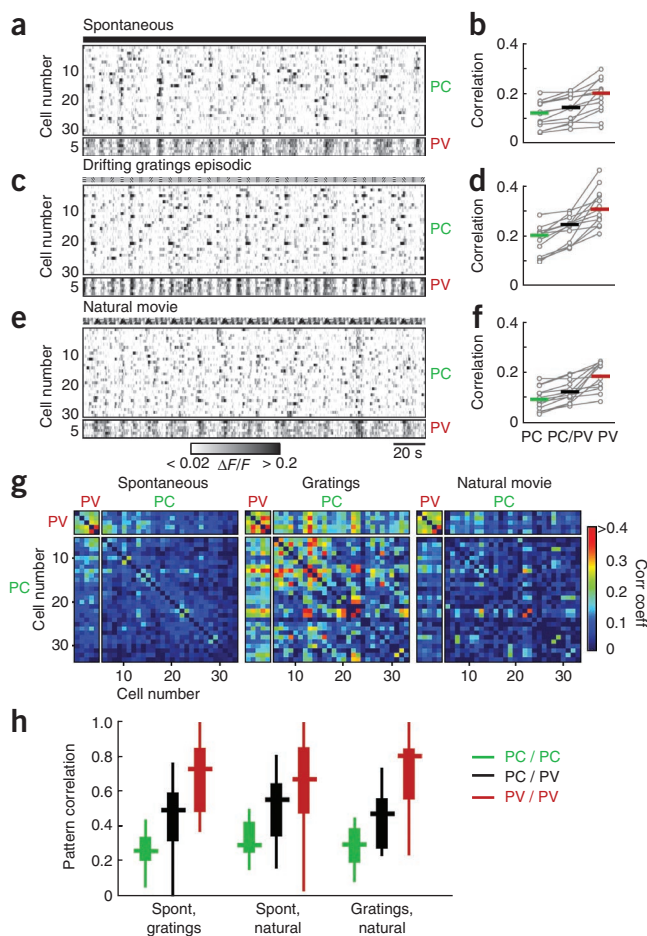
$R = 0.20$ ; group medians of imaged regions,  $P = 0.005$ , sign rank test; **Fig. 4b,d**). By contrast, continuously presented natural movies significantly decorrelated the responses of pyramidal cells (natural:  $R = 0.09$ ,  $P = 0.007$ ; **Fig. 4e,f**).

Between PV neurons, time-varying response correlations were on average considerably stronger than between pyramidal cells during all conditions (spontaneous:  $R = 0.20$ ; gratings:  $R = 0.31$ ; natural:  $R = 0.18$ ; group median of imaged regions,  $P < 0.0005$ ; **Fig. 4b,d,f**), and during visual stimulation even stronger than correlations between PV neurons and the surrounding neuropil (**Supplementary Fig. 6**). Pairs consisting of one pyramidal cell and one PV cell showed intermediate correlation strength during all conditions (**Fig. 4b,d,f**). Together, these

we tested the similarity between spontaneous activity patterns and those evoked by different types of visual stimulus by presenting both episodically drifting whole-field gratings and sequences of naturalistic movies (**Fig. 4a–f**; see Online Methods).

Spontaneous activity was characterized by brief (<1 s), sporadic events involving multiple neurons, separated by periods in which few neurons were active (**Fig. 4a**). The presentation of visual stimuli resulted in reproducible patterns of activity and changed network activity in different ways: episodically presented drifting gratings induced epochs of many active neurons (**Fig. 4c**, corresponding to the periods of grating drift) alternated with periods of almost complete lack of activity in the population (corresponding to periods of no drift). This strong periodic recruitment of the circuit caused the overall strength of time-varying response correlations (total correlations) of calcium signals between pyramidal cells to increase compared to those during spontaneous activity (spontaneous:  $R = 0.12$ ; gratings:

**Figure 4** Comparison of population activity patterns with and without visual stimulation. **(a,c,e)** Calcium signals of 30 pyramidal cells (PCs, top) and 6 PV neurons (bottom) simultaneously imaged in darkness with the monitor switched off **(a)**, during stimulation with episodically drifting gratings **(c)** or with natural movie sequences **(e)**. Schematic of stimulus sequence is shown above each plot. **(b,d,f)** Strength of pair-wise time-varying (total) correlations from calcium signals for pyramidal cell pairs (left), PV cell pairs (right) and mixed pyramidal cell–PV cell pairs (middle) during spontaneous activity **(b)**, visual stimulation with gratings **(d)** or natural movies **(f)**. Circles, median values of each imaged region; colored lines, group medians. Gray lines connect values from the same imaged region. **(g)** Matrices of pair-wise response rate correlation coefficients between significantly responsive PV and pyramidal cells of one imaged region. Cells were ordered such that the strongest correlations during spontaneous activity were close to the diagonal in the spontaneous condition, and the same order was applied to correlation matrices of the other conditions. Positions on the diagonal were set to the lowest value. **(h)** The similarity between two matrices is the correlation coefficient of their off-diagonal elements (pattern correlation). Comparisons were made between correlation matrices of spontaneous and each of the evoked conditions and between different visually evoked conditions for pyramidal cells (green), PV cells (red) and for matrices from mixed pyramidal cell–PV cell pairs (black). Boxplots of pattern correlation values of all imaged regions that included three or more responsive PV cells (horizontal lines are group medians, 6 animals, 13 regions).



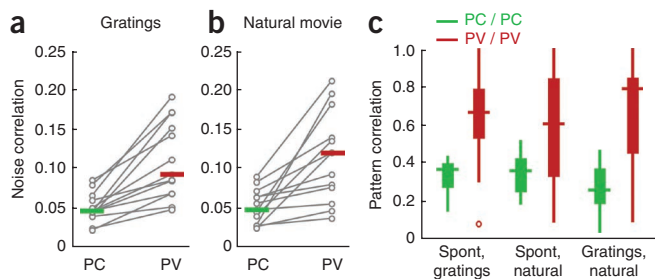


**Figure 5** Comparison between spontaneous and noise correlation patterns during visual stimulation. **(a,b)** Noise correlation coefficients from calcium signals during stimulation with drifting gratings **(a)** or with natural movie sequences **(b)** for pyramidal cell pairs (left, green) and PV cell pairs (right, red). Circles, median values for each region; colored lines, group medians. **(c)** Boxplots of similarity of matrices of noise correlations during visually evoked conditions (see Online Methods) and correlations during spontaneous activity (left and middle), and similarity of noise correlation matrices during grating and natural movie stimulation (right) for pyramidal cell (green) and PV cell (red) populations. Pattern correlation values are correlation coefficients of off-diagonal matrix elements for each imaged region with three or more responsive PV cells; 6 animals, 13 regions. Insert, horizontal lines are median values.

results are consistent with the connectivity profile of pyramidal cells and PV cells in the local circuit: PV cells share more common input (Fig. 2) and are more interconnected<sup>42,43</sup>, and therefore show more correlated activity.

To test whether neurons tended to be similarly co-active or co-inactive during spontaneous activity and during visual stimulation, we determined how the structure of correlations of pyramidal cell or PV cell populations changed across stimulus conditions. We computed matrices of pair-wise correlations for all cell pairs in one imaged region from recordings of spontaneous activity and during stimulation with episodically drifting gratings or natural movies (Fig. 4g). If neuronal ensembles that fire together without visual input are also likely to be co-active during visual stimulation, correlation matrices for the different conditions would look similar. This was the case for populations of PV interneurons, but not for pyramidal cells (Fig. 4g). To obtain a quantitative measure of similarity between spontaneous and sensory-evoked co-activation patterns, we calculated the correlation coefficient of the off-diagonal elements between the different matrices, which we term pattern correlation (Fig. 4h). When comparing correlations between pyramidal cells across imaged regions, we found that visual stimulation strongly altered correlation patterns during periods of spontaneous activity (Fig. 4h and Supplementary Fig. 7, group median pattern correlation: spontaneous versus gratings, 0.27; spontaneous versus natural movie, 0.30). We found equally large differences in correlation patterns when we compared population activity driven by different stimuli (Fig. 4h and Supplementary Fig. 7, group median pattern correlation: gratings versus natural movie, 0.30). Therefore, there seems to be only a weak resemblance between patterns of pyramidal cell co-activation during spontaneous activity and different stimulus regimes. This suggests that biased local connectivity does not strongly influence how pyramidal cell populations respond to external input, which allows individual neurons to participate in different ensembles.

By contrast, the degree of correlated activity between pairs of PV cells was largely maintained regardless of whether they were active spontaneously or driven by a visual stimulus (Fig. 4g,h). If two PV cells were strongly correlated during one stimulus condition, they were likely to be strongly correlated in another. Thus, although the

patterns of correlated activity among pyramidal cells were different between spontaneous and different visually evoked states, the co-activation patterns in networks of PV cells were very similar (Fig. 4h and Supplementary Fig. 7; group median pattern correlation: spontaneous versus gratings, 0.73; spontaneous versus natural movie, 0.67; gratings versus natural movie, 0.80). Pattern correlations for pairs consisting of one pyramidal cell and one PV cell showed intermediate values (Fig. 4h; group median pattern correlation >0.47 across all conditions), indicating that the groups of pyramidal cells associated with the firing of PV neurons tended to change during different conditions, but not as much as the co-activation patterns in populations of pyramidal cells. Calculating pattern correlations across different conditions from inferred spikes instead of the raw calcium signals produced similar results (Supplementary Fig. 8).

Together, these results indicate that the patterns of network co-activation of pyramidal cells were more strongly influenced by visual input than the co-activation patterns of PV cells, which appeared similar across conditions. This suggests that the activity of PV cells was strongly determined by intrinsic connectivity.

### Structure of noise correlations

Although biased recurrent connectivity might not dominate response patterns of pyramidal cells, it could still influence them. The differences in total correlations described above do not show whether changes in co-activation patterns are a result of a change in feedforward input due to different stimuli or a change in the state of network activity due to regrouping of local ensembles. To test this, we separated the total correlations between cell pairs into signal and noise components: signal correlations arise from correlations in the stimulus itself or similarity in preferred stimulus features (such as orientation), whereas noise correlations arise from mutual connectivity or shared inputs that are reflected in the trial-to-trial variability of responses. Noise correlations were much higher for pairs of PV cells than for pairs of pyramidal cells ( $P < 0.001$  for all comparisons; Fig. 5a,b). The magnitude of average noise correlations for each group of cell pairs was not different between the two visual stimulation protocols ( $P > 0.3$  for all comparisons; Fig. 5a,b).

Comparing the pattern of noise correlations between different stimulus conditions to the pattern of spontaneous correlations allowed us to investigate whether the extensive restructuring of pyramidal cell co-activations (Fig. 4h) arose primarily from changes in stimulus-evoked response patterns (signal correlation) or also from changes in the structure of noise correlation. For pyramidal cells, the pattern of pair-wise noise correlations in the population was relatively different from spontaneous correlation patterns for both stimulus conditions (group median pattern correlation spontaneous versus gratings, 0.37; spontaneous versus natural movie, 0.36; Fig. 5c), whereas for PV cells the pattern of noise correlations was more similar (group median pattern correlation spontaneous versus gratings, 0.66; spontaneous versus natural movie, 0.60; Fig. 5c). In fact, for both pyramidal cell and PV cell populations the similarity of noise correlation patterns (Fig. 5c) was not significantly different from that obtained from total pair-wise correlations ( $P > 0.08$  for all comparisons; Fig. 4h).

For pyramidal cells, the differences in patterns of noise correlation and spontaneous correlation indicate that even the component of co-activation patterns that is not directly evoked by the visual stimulus is different from spontaneous co-activation patterns. Moreover, the structure of pyramidal cell–pyramidal cell noise correlations also changed between grating stimuli and natural movies (group median pattern correlation, 0.26; Fig. 5c), suggesting that different types of

feedforward input not only regroup the local population of pyramidal cells into different ensembles, but also place the local circuit into very different activity states with changed network interactions. PV cells, in contrast, behaved differently: their co-activation patterns were largely maintained in the absence or presence of feedforward input.

## DISCUSSION

We found fundamental differences in synaptic connectivity, visual response properties and network dynamics between populations of layer 2/3 excitatory pyramidal cells and inhibitory fast-spiking PV interneurons in mouse V1. Co-activations of sparsely but selectively connected pyramidal cells depended strongly on stimulus identity, and only weakly reflected biased local connectivity. By contrast, the pattern of co-activations of densely connected and more broadly tuned fast-spiking PV cells depended weakly on visual input, and seemed largely to reflect local network activity.

The contribution of inhibition during sensory processing in V1 will depend crucially on the tuning properties of interneurons. There is considerable debate about the selectivity of fast-spiking PV interneurons, which provide rapidly acting, soma-targeted inhibition of pyramidal cells<sup>1,20–22</sup>. We used cell-attached recordings and two-photon calcium imaging in mice expressing tdTomato in PV neurons, which mostly comprised fast-spiking cells, and found that their calcium signals reliably reflected changes in firing rate. We found that fast-spiking PV cells showed a range of tuning widths. Although a small subset of cells was more selective for stimulus orientation, most were more broadly tuned (Fig. 1). This result was confirmed in both wild-type and PV-tdTomato mice by *in vitro* electrophysiological identification of fast-spiking cells, whose orientation tuning had been functionally characterized *in vivo* (Fig. 2).

The broader tuning of most fast-spiking PV cells in mice is consistent with their synaptic connectivity profile in the local network. We found that fast-spiking interneurons received highly dense, local excitatory connections (see also ref. 23) that were on average an order of magnitude stronger than connections between pyramidal cells. We found this arrangement of pyramidal cell–fast-spiking cell connections to be much denser than in rat visual cortex<sup>7</sup>, which could reflect either a difference between species or a consequence of there being fewer severed connections between neurons because we recorded deeper in the slice. In combined *in vivo* and *in vitro* experiments on the same tissue, we have shown directly that predominantly broadly tuned fast-spiking PV cells indiscriminately sample strong inputs from a local population of pyramidal cells with a diverse range of orientation preference and selectivity. Our data support the idea that local inhibition in V1 is recruited nonspecifically and primarily reflects the strength of firing in the local network<sup>20</sup>, but argues against distinct subnetworks of excitatory and inhibitory neurons sharing the same preference for visual features<sup>10,22</sup>. Our results also lead to a prediction for the width of orientation tuning of fast-spiking interneurons in carnivore V1 which, unlike in mice, contains functional columns: given similarly dense pyramidal cell–fast-spiking cell connectivity, the tuning of fast-spiking cell neurons is expected to be narrow in iso-orientation domains, but broader in pinwheel centers, which may explain mixed reports regarding the selectivity of fast-spiking neurons in cats<sup>16–18</sup>.

How do these fundamental differences in synaptic connectivity and feature selectivity of pyramidal cells and fast-spiking PV cells relate to their network dynamics? Neuronal responses during sensory processing are likely to be influenced by both the intrinsic organization of intracortical connections and the statistical features of sensory stimuli that provide the main feedforward drive to the cortical circuit.

The extent to which these intrinsic and extrinsic factors dominate cortical activity is still not resolved. On one hand, several reports have suggested that patterns of evoked activity resemble those occurring spontaneously, and that the structure of neuronal correlations remains similar irrespective of the presence or absence of a sensory drive<sup>24–29</sup>. On the other hand, other studies have reported that sensory stimuli or changes in brain state can alter the strength of neuronal correlations and network interactions<sup>30–32,44–46</sup>. The different extents to which sensory input restructures patterns of cortical network activity as reported by different studies could be attributed to various factors other than cell type such as differences in animal species, cortical areas, cortical layers and the spatial scale, coverage and resolution of the methods used. Although our study cannot account for all these factors, our data make a clear distinction between the behavior of layer 2/3 pyramidal cell and fast-spiking PV cell assemblies.

In populations consisting of inhibitory fast-spiking PV cells, correlations in both overall activity and trial-to-trial variability were similar during periods of spontaneous and visually evoked activity. This agrees with the very dense sampling of local excitatory connections by fast-spiking PV cells, such that nearby PV cells share a substantial amount of common input, and are therefore more correlated than those separated by greater distances (Supplementary Fig. 5). These results are also consistent with the observation that spontaneously occurring action potentials of neighboring fast-spiking cells in mouse somatosensory cortex are synchronized and are driven by highly correlated depolarizations<sup>44</sup>. Membrane potential synchronization might also be augmented by electrical coupling<sup>42,43</sup>. Therefore, the co-activation patterns of neighboring fast-spiking PV cells are not strongly altered by sensory drive. Instead, the weak stimulus dependence of fast-spiking PV cell correlations is consistent with the notion that the activity of these interneurons is largely dominated by local activity in the network. Although neighboring fast-spiking PV neurons might also receive selective feedforward or long-range excitatory connections, these inputs are apparently not sufficient to substantially decorrelate their firing (on the scale of hundreds of milliseconds).

In populations of pyramidal cells, we found a very weak relationship between the similarity of visual responses (signal correlation) and the magnitude of spontaneous firing rate correlations, suggesting that neurons that prefer similar visual features tended to be only slightly more co-active spontaneously than neurons that do not. The structure of both firing rate (total) and noise correlations was only weakly related between the spontaneous state and during presentation of drifting gratings and naturalistic movies, indicating that the same neuronal subsets were rarely similarly co-active during these conditions. These results suggest that the cortical representation of a visual stimulus in pyramidal cell populations does not strongly reflect the existing biases of their recurrent connectivity. As the connections between nearby pyramidal cells in layer 2/3 are both sparse and weak (Fig. 2), the fraction of shared local input between a pair of pyramidal cells is likely to be small, allowing feedforward or other inputs to influence and potentially to decorrelate their firing. At present, however, it is not possible to identify the main sources of correlated variability of pyramidal cells beyond ruling out a dominant role of biased local connections, whose influence may be additionally attenuated by active mechanisms of decorrelation<sup>33,35</sup>. Our data support the idea that regrouping of pyramidal cells into different ensembles is strongly governed by the statistics of sensory input, which is consistent with reports on the state- or stimulus-dependence of neuronal interactions<sup>30–32,44,45</sup>.

These data reveal fundamentally different operational regimes of excitatory and inhibitory neurons during sensory processing. Similar patterns of co-activation of fast-spiking PV cells across stimulus

conditions contrasted with the strong dependence of pyramidal cell co-activations on sensory drive, which allows unique stimuli to be represented by unique pyramidal cell response patterns. These attributes of pyramidal cell activity might offer substantial advantages for sensory coding, as ensembles of pyramidal cells are much more informative about the identity of a stimulus than are fast-spiking PV cells (**Supplementary Fig. 9**). Thus, in a sparsely active local network composed of pyramidal cells with diverse receptive fields, the variability and independence of responses might reduce local activity correlations and improve the efficiency of population coding<sup>34,47</sup>.

## METHODS

Methods and any associated references are available in the online version of the paper at <http://www.nature.com/natureneuroscience/>.

*Note: Supplementary information is available on the Nature Neuroscience website.*

## ACKNOWLEDGMENTS

We thank T. Margrie, A. Arenz and E. Rancz for help with *in vivo* electrophysiology, J. Sjöström and K. Buchanan for help with *in vitro* electrophysiology, J. Rothman for NeuroMatic software, and M. Hübener and M. Sahani for comments on an earlier version of this manuscript. This work was supported by the Wellcome Trust (T.D.M.-F.), the European Research Council (T.D.M.-F.), the European Molecular Biology Organization (S.B.H.) and the Humboldt Foundation (S.B.H.). We also received funding from the European Community's Seventh Framework Programme (FP2007-2013) under grant agreement no. 223326 (T.D.M.-F.).

## AUTHOR CONTRIBUTIONS

S.B.H. and H.K. performed all *in vivo* and slice experiments. S.B.H., H.K., N.A.L. and T.D.M.-F. analyzed the data. H.R. carried out antibody labeling. B.P. developed software for visual stimulation, image acquisition and image analysis. J.V. developed spike inference algorithms. E.L. and H.Z. generated and supplied the mice. S.B.H., H.K., N.A.L. and T.D.M.-F. wrote the paper.

## COMPETING FINANCIAL INTERESTS

The authors declare no competing financial interests.

Published online at <http://www.nature.com/natureneuroscience/>.

Reprints and permissions information is available online at <http://www.nature.com/reprints/index.html>.

- Markram, H. *et al.* Interneurons of the neocortical inhibitory system. *Nat. Rev. Neurosci.* **5**, 793–807 (2004).
- Gonchar, Y., Wang, Q. & Burkhalter, A. Multiple distinct subtypes of GABAergic neurons in mouse visual cortex identified by triple immunostaining. *Front. Neuroanat.* **1**, 3 (2007).
- Sillito, A.M. The contribution of inhibitory mechanisms to the receptive field properties of neurones in the striate cortex of the cat. *J. Physiol. (Lond.)* **250**, 305–329 (1975).
- Priebe, N.J. & Ferster, D. Inhibition, spike threshold, and stimulus selectivity in primary visual cortex. *Neuron* **57**, 482–497 (2008).
- Ozeki, H., Finn, I.M., Schaffer, E.S., Miller, K.D. & Ferster, D. Inhibitory stabilization of the cortical network underlies visual surround suppression. *Neuron* **62**, 578–592 (2009).
- Liu, B. *et al.* Intervening inhibition underlies simple-cell receptive field structure in visual cortex. *Nat. Neurosci.* **13**, 89–96 (2010).
- Holmgren, C., Harkany, T., Svennenfors, B. & Zilberter, Y. Pyramidal cell communication within local networks in layer 2/3 of rat neocortex. *J. Physiol. (Lond.)* **551**, 139–153 (2003).
- Thomson, A.M. & Lamy, C. Functional maps of neocortical local circuitry. *Front. Neurosci.* **1**, 19–42 (2007).
- Oswald, A.-M.M., Doiron, B., Rinzel, J. & Reyes, A.D. Spatial profile and differential recruitment of GABA<sub>A</sub> modulate oscillatory activity in auditory cortex. *J. Neurosci.* **29**, 10321–10334 (2009).
- Yoshimura, Y. & Callaway, E.M. Fine-scale specificity of cortical networks depends on inhibitory cell type and connectivity. *Nat. Neurosci.* **8**, 1552–1559 (2005).
- Ko, H. *et al.* Functional specificity of local synaptic connections in neocortical networks. *Nature* **473**, 87–91 (2011).
- Yoshimura, Y., Dantzker, J.L.M. & Callaway, E.M. Excitatory cortical neurons form fine-scale functional networks. *Nature* **433**, 868–873 (2005).
- Gilbert, C.D. & Wiesel, T.N. Columnar specificity of intrinsic horizontal and corticocortical connections in cat visual cortex. *J. Neurosci.* **9**, 2432–2442 (1989).
- Alonso, J.M., Usrey, W.M. & Reid, R.C. Rules of connectivity between geniculate cells and simple cells in cat primary visual cortex. *J. Neurosci.* **21**, 4002–4015 (2001).
- Alonso, J.M. & Martinez, L.M. Functional connectivity between simple cells and complex cells in cat striate cortex. *Nat. Neurosci.* **1**, 395–403 (1998).
- Hirsch, J.A. *et al.* Functionally distinct inhibitory neurons at the first stage of visual cortical processing. *Nat. Neurosci.* **6**, 1300–1308 (2003).
- Cardin, J.A., Palmer, L.A. & Contreras, D. Stimulus feature selectivity in excitatory and inhibitory neurons in primary visual cortex. *J. Neurosci.* **27**, 10333–10344 (2007).
- Nowak, L.G., Sanchez-Vives, M.V. & McCormick, D.A. Lack of orientation and direction selectivity in a subgroup of fast-spiking inhibitory interneurons: cellular and synaptic mechanisms and comparison with other electrophysiological cell types. *Cereb. Cortex* **18**, 1058–1078 (2008).
- Sohya, K., Kameyama, K., Yanagawa, Y., Obata, K. & Tsumoto, T. GABAergic neurons are less selective to stimulus orientation than excitatory neurons in layer II/III of visual cortex, as revealed by *in vivo* functional Ca<sup>2+</sup> imaging in transgenic mice. *J. Neurosci.* **27**, 2145–2149 (2007).
- Kerlin, A.M., Andermann, M.L., Berezovskii, V.K. & Reid, R.C. Broadly tuned response properties of diverse inhibitory neuron subtypes in mouse visual cortex. *Neuron* **67**, 858–871 (2010).
- Ma, W. *et al.* Visual representations by cortical somatostatin inhibitory neurons—selective but with weak and delayed responses. *J. Neurosci.* **30**, 14371–14379 (2010).
- Runyan, C.A. *et al.* Response features of parvalbumin-expressing interneurons suggest precise roles for subtypes of inhibition in visual cortex. *Neuron* **67**, 847–857 (2010).
- Bock, D.D. *et al.* Network anatomy and *in vivo* physiology of visual cortical neurons. *Nature* **471**, 177–182 (2011).
- Tsodyks, M., Kenet, T., Grinvald, A. & Arieli, A. Linking spontaneous activity of single cortical neurons and the underlying functional architecture. *Science* **286**, 1943–1946 (1999).
- Ch'ng, Y.H. & Reid, R.C. Cellular imaging of visual cortex reveals the spatial and functional organization of spontaneous activity. *Front. Integr. Neurosci.* **4**, 20 (2010).
- Fiser, J., Chiu, C. & Weliky, M. Small modulation of ongoing cortical dynamics by sensory input during natural vision. *Nature* **431**, 573–578 (2004).
- MacLean, J.N., Watson, B.O., Aaron, G.B. & Yuste, R. Internal dynamics determine the cortical response to thalamic stimulation. *Neuron* **48**, 811–823 (2005).
- Luczak, A., Barthó, P. & Harris, K.D. Spontaneous events outline the realm of possible sensory responses in neocortical populations. *Neuron* **62**, 413–425 (2009).
- Jermakowicz, W.J., Chen, X., Khaytin, I., Bonds, A.B. & Casagrande, V.A. Relationship between spontaneous and evoked spike-time correlations in primate visual cortex. *J. Neurophysiol.* **101**, 2279–2289 (2009).
- Smith, M.A. & Kohn, A. Spatial and temporal scales of neuronal correlation in primary visual cortex. *J. Neurosci.* **28**, 12591–12603 (2008).
- Kohn, A. & Smith, M.A. Stimulus dependence of neuronal correlation in primary visual cortex of the macaque. *J. Neurosci.* **25**, 3661–3673 (2005).
- Nauhaus, I., Busse, L., Carandini, M. & Ringach, D.L. Stimulus contrast modulates functional connectivity in visual cortex. *Nat. Neurosci.* **12**, 70–76 (2009).
- Renart, A. *et al.* The asynchronous state in cortical circuits. *Science* **327**, 587–590 (2010).
- Ecker, A.S. *et al.* Decorrelated neuronal firing in cortical microcircuits. *Science* **327**, 584–587 (2010).
- Ohiorhenuan, I.E. *et al.* Sparse coding and high-order correlations in fine-scale cortical networks. *Nature* **466**, 617–621 (2010).
- Stosiek, C., Garaschuk, O., Holthoff, K. & Konnerth, A. *In vivo* two-photon calcium imaging of neuronal networks. *Proc. Natl. Acad. Sci. USA* **100**, 7319–7324 (2003).
- Ohki, K., Chung, S., Ch'ng, Y.H., Kara, P. & Reid, R.C. Functional imaging with cellular resolution reveals precise micro-architecture in visual cortex. *Nature* **433**, 597–603 (2005).
- Mrsic-Flogel, T.D. *et al.* Homeostatic regulation of eye-specific responses in visual cortex during ocular dominance plasticity. *Neuron* **54**, 961–972 (2007).
- Madisen, L. *et al.* A robust and high-throughput Cre reporting and characterization system for the whole mouse brain. *Nat. Neurosci.* **13**, 133–140 (2010).
- Vogelstein, J.T. *et al.* Fast nonnegative deconvolution for spike train inference from population calcium imaging. *J. Neurophysiol.* **104**, 3691–3704 (2010).
- Niell, C.M. & Stryker, M.P. Highly selective receptive fields in mouse visual cortex. *J. Neurosci.* **28**, 7520–7536 (2008).
- Galarreta, M. & Hestrin, S. A network of fast-spiking cells in the neocortex connected by electrical synapses. *Nature* **402**, 72–75 (1999).
- Gibson, J.R., Beierlein, M. & Connors, B.W. Two networks of electrically coupled inhibitory neurons in neocortex. *Nature* **402**, 75–79 (1999).
- Genet, L.J., Avermann, M., Matyas, F., Staiger, J.F. & Petersen, C.C.H. Membrane potential dynamics of GABAergic neurons in the barrel cortex of behaving mice. *Neuron* **65**, 422–435 (2010).
- Zohary, E., Shadlen, M.N. & Newsome, W.T. Correlated neuronal discharge rate and its implications for psychophysical performance. *Nature* **370**, 140–143 (1994).
- Poulet, J.F.A. & Petersen, C.C.H. Internal brain state regulates membrane potential synchrony in barrel cortex of behaving mice. *Nature* **454**, 881–885 (2008).
- Chelaru, M.I. & Dragoi, V. Efficient coding in heterogeneous neuronal populations. *Proc. Natl. Acad. Sci. USA* **105**, 16344–16349 (2008).

## ONLINE METHODS

**Animals and surgical procedures.** All experimental procedures were carried out in accordance with institutional animal welfare guidelines and licensed by the UK Home Office. Experiments were performed on C57Bl/6 mice or PV-Cre × Isl-tdTomato transgenic mice. Generation and characterization of the PV-Cre-Isl-tdTomato transgenic mouse line was as described<sup>39</sup> (original name: Pvalb-2A-Cre;Ai9). Briefly, the PV-Cre mouse line was generated by constructing a targeting vector in which the T2A-Cre sequence was fused in-frame to the 3' end of the parvalbumin coding sequence, transfecting the targeting vector into the G4 129/B6 F1 hybrid embryonic stem cell line, and selecting properly recombined embryonic stem cell clones to produce the mouse line. The PV-Cre mice were then crossed with the Ai9 Isl-tdTomato reporter line<sup>39</sup> to produce the double transgenic PV-Cre-Isl-tdTomato mice for experiments.

Mice were initially anesthetized with a mixture of Fentanyl (0.05 mg per kg of body weight), Midazolam (5.0 mg per kg) and Medetomidin (0.5 mg per kg). At the time of imaging, the injectable anesthetic had mostly worn off and light anesthesia was maintained by isoflurane (0.3–0.5%, vol/vol) in a 60:40 mixture of O<sub>2</sub>:N<sub>2</sub>O delivered through a small nose cone. Surgery was performed as described<sup>38</sup>. Briefly, a small craniotomy (1–2 mm) was performed over V1 and sealed after dye injection with 1.6% agarose in Hepes-buffered artificial cerebrospinal fluid (ACSF) and a cover slip.

**Dye loading and two-photon imaging.** For bulk loading of cortical neurons<sup>36</sup> the calcium-sensitive dye Oregon Green Bapta-1 AM (OGB-1 AM, Molecular Probes) was first dissolved in 4 μl DMSO containing 20% Pluronic F-127 (wt/vol, Molecular Probes), and further diluted (1/11) in dye buffer (150 mM NaCl, 2.5 mM KCl, and 10 mM HEPES (pH 7.4)) to yield a final concentration of 0.9 mM. Sulforhodamine 101 (50 μM, Molecular Probes) was added to the solution for experiments in C57Bl/6 mice to distinguish neurons and astrocytes<sup>48</sup>. The dye was slowly pressure-injected into the right visual cortex at a depth of 170–200 μm with a micropipette (3–5 MΩ, 3–10 p.s.i., 2–4 min) under visual control by two-photon imaging (10× water immersion objective, Olympus). The activity of cortical neurons was monitored by imaging fluorescence changes with a custom-built microscope and a mode-locked Ti:sapphire laser (Mai Tai, Spectra-Physics) at 830 nm or 930 nm through a 40× water immersion objective (0.8 NA, Olympus). Scanning and image acquisition were controlled by custom software written in LabVIEW (National Instruments).

**In vivo cell-attached recordings.** Loose-seal cell-attached recordings *in vivo* were performed on OGB-1 loaded neurons in layer 2/3 with micropipettes of 4–7 MΩ, pipette solution containing (in mM): 150 NaCl, 2.5 KCl, 10 Hepes, 1 MgCl<sub>2</sub>, 1 CaCl<sub>2</sub> (300 mOsm) and 25 μM Alexa Fluor 594. The craniotomy was covered with agar. Neurons were targeted visually with two-photon imaging at 830 or 930 nm. Signals were recorded using an ELC-03XS amplifier (NPI) and Igor Pro NClamp/Neuromatic software (J. Rothman, UCL), bandpass filtered between 0.3 and 5 kHz and digitized at 10 kHz.

**Visual stimulation.** Visual stimuli were generated using MATLAB (MathWorks) Psychophysics Toolbox<sup>49</sup>, and displayed on a LCD monitor (60 Hz refresh rate) positioned 20 cm from the left eye, roughly at 45° to the long axis of the animal, covering ~105 × 85° of visual space. At the beginning of each experiment, the appropriate retinotopic position in visual cortex was determined using small grating stimuli at 12–24 neighboring positions. Only cortical regions in the monocular part of V1 were included in the analysis. The monitor was repositioned such that the preferred retinotopic position of most imaged neurons was roughly in the middle of the monitor. Calcium signals were measured in the dark (monitor and room lights turned off) for 6–12 min and in response to sequences of full-field grating stimuli and natural movies. Square wave gratings (0.035 cycles per deg, 2 cycles per s) drifting in eight different directions were shown episodically at 100% contrast, with the grating standing for 4 s (occasionally, a gray screen was used instead of the standing grating) before moving for 2 s (eight stimulus repetitions). Naturalistic movies consisted of 16-s sequences of either moving scenes in a mouse cage or compilations of David Attenborough's Life of Mammals (BBC), adjusted to 70% mean contrast, continuously looped 19 times. The first stimulus repetition was removed from analysis to exclude onset-related responses. For the functional characterization of neurons before *in vitro* connectivity mapping, square wave gratings drifting in eight different

directions were randomly interleaved, with the grating standing for 1.4–1.9 s before moving for 0.9–1.5 s (6–8 repetitions per grating).

**Data acquisition and analysis.** Imaging frames of 256 × 256 pixels or 256 × 128 pixels were acquired at 7.6 or 15.2 Hz, respectively. Image sequences recorded at 15.2 Hz were subsequently resampled to 7.6 Hz. After each recording the focal plane and imaging position were checked and realigned with the initial image if necessary. Image sequences were aligned for tangential drift and analyzed with custom programs written in ImageJ (NIH), MATLAB and LabVIEW. Cell outlines were detected using a semi-automated algorithm based on cell intensity, size and shape, and confirmed by visual inspection. After erosion of the cell-based regions of interest (ROIs) (to minimize influence of the neuropil signal around the cell bodies) all pixels within each ROI were averaged to give a single time course ( $\Delta F/F$ ), which was additionally highpass filtered at a cutoff frequency of 0.02 Hz to remove slow fluctuations in the signal. Nonresponsive neurons were excluded from further analysis by testing whether, for each cell, a significant calcium response was observed relative to baseline for at least one grating direction and for one or more frames of the natural movie sequence (one-way ANOVA,  $P < 0.0001$ ).

To determine neuronal response preferences to drifting gratings from average responses for *in vivo* to *in vitro* connectivity mapping experiments, we inferred spike trains from calcium signals using a fast, non-negative deconvolution method that approximates the most likely spike train for each neuron, given the fluorescence observations<sup>40</sup>. This method yields spike probabilities that approximate the number of action potentials per imaging frame, or inferred firing rate. For pyramidal neurons,  $\tau$  (decay constant of calcium transients) was set to 0.8 s, and the calcium signal baseline was the mean of all values from the calcium trace. For PV neurons  $\tau$  was set to 2 s, and the baseline was determined as the tenth percentile of all values. These settings resulted in the best correspondence between inferred spike probability and real spike rate measured during simultaneous calcium imaging and cell-attached recordings (Supplementary Figs. 2 and 4; 16 pyramidal cells from 7 mice, 12 PV cells from 6 mice). For pyramidal neurons inferred spike probabilities of 0.022 or less, and for PV cells probabilities of 0.008 or less, were typically not associated with actual spikes, and were therefore set to 0. To relate inferred spiking probability to actual spike rate for pyramidal neurons (Supplementary Fig. 2f), we attributed empirically recorded spikes to inferred spiking values if they occurred with a time difference  $\Delta t < 195$  ms and were not already assigned to a previous inferred spike. The average calcium signal from the same time window shifted by one bin was taken to compare calcium transient amplitude and real spike rate (Supplementary Fig. 2e). The algorithm detected 100% of bursts of three or more spikes,  $95 \pm 2\%$  (mean  $\pm$  s.e.m.) of bursts of two spikes and  $53 \pm 6\%$  of single spikes, with a false-positive rate of  $0.049 \pm 0.009$  Hz. As PV cells showed on average much higher spike rates, spikes were not attributed to inferred spikes, but inferred spiking values or real spikes were summed, and the calcium signal averaged in time bins of 393 ms for comparison (Fig. 1d,e and Supplementary Fig. 4c,d). For PV cells the algorithm detected  $92 \pm 2\%$  of all spikes with a false-positive rate of  $0.25 \pm 0.03$  Hz. As spike rates were much higher for PV cells than for pyramidal cells (average spike rate during stimulation with episodically drifting gratings for pyramidal neurons:  $0.57 \pm 0.09$  Hz; PV neurons:  $8.2 \pm 1.8$  Hz), false positive rates as a fraction of total spike count were roughly similar for the two cell types.

Among cells that were responsive to grating stimuli, the average firing rate, average inferred firing rate or average calcium signal over the duration of grating drift was taken as the response to each grating stimulus. Responses from different trials were averaged to obtain the orientation tuning curve. This orientation tuning curve was then Fourier interpolated to 360 points, and the preferred direction was determined by the angle at which the interpolated tuning curve attained its maximum. The preferred orientation was taken as the modulus of the preferred direction to 180°. OSI was calculated as  $(R_{\text{best}} - R_{\text{ortho}})/(R_{\text{best}} + R_{\text{ortho}})$ , where  $R_{\text{best}}$  is the interpolated response to the best direction and  $R_{\text{ortho}}$  is the average of interpolated responses to the directions orthogonal to the best direction.

**Correlations, pattern correlations and matrix reordering.** Pair-wise correlations were calculated using Pearson's correlation coefficient from the calcium signals of two cells over the duration of the whole recording (total correlation). Signal correlation was calculated from average responses across trials of drifting gratings or natural movies, and noise correlations were determined by subtracting



the average response from the responses in each trial and calculating the correlation coefficient of the mean-subtracted response over the time course of the recording. For **Figure 3d**, correlation coefficients of all cell pairs from each imaged region were first z-scored (each value was normalized by subtracting the population mean of the imaged region and dividing by the variance), before pooling the data from all the regions in a single plot.

For visual comparison, the correlation coefficients were displayed in matrix form (**Fig. 4g**), where each element is the correlation coefficient for a pair of neurons. Neurons were ordered such that the strongest values were close to the diagonal for one stimulus condition; we used a search algorithm to maximize the Frobenius inner product between the actual pairwise correlation matrix and a Toeplitz matrix whose values decay exponentially from the diagonal<sup>28</sup>. To aid direct visual comparison, this ordering was applied to the correlation matrices of other conditions. The similarity between two matrices (pattern correlation) is the correlation coefficient of their off-diagonal elements.

**Immunocytochemical and electrophysiological characterization of layer 2/3 PV neurons.** For immunocytochemical analysis, transgenic animals were perfused with 4% paraformaldehyde (wt/vol) in phosphate-buffered saline and 50- $\mu$ m-thick coronal slices were obtained from the visual cortex. Free-floating sections were incubated (4 °C, 48 h) in phosphate-buffered saline and Triton X-100 (0.2%, vol/vol) solution containing primary antibodies against parvalbumin (mouse anti-parvalbumin, 1:1,000, Swant #PV235). Fluorescent conjugates were used to visualize parvalbumin immunoreactivity (AlexaFluor 488-conjugated goat anti-mouse, 1:1,000, 4 °C overnight, Invitrogen). Primary and secondary antibodies were initially tested for optimal dilution. Mounted sections were analyzed using two-photon scanning microscopy at 930 nm wavelength, with a filter set suitable for separating AlexaFluor 488 and tdTomato fluorescence emission. In superficial layers (<200  $\mu$ m from the pial surface), which correspond to the regions recorded during *in vivo* calcium imaging, tdTomato was coexpressed with parvalbumin in 92% of the tdTomato-expressing cells (88 out of 96) and in 100% of the parvalbumin-positive cells (**Supplementary Fig. 1f**). In deeper layers, however, the colocalization was poorer (**Supplementary Fig. 1f**), possibly owing to expression of parvalbumin in some layer 5 pyramidal neurons during development<sup>50</sup>.

Three adult PV-Cre-lsl-tdTomato mice were used for electrophysiological characterization of PV neurons. The mouse brain was removed and dissected rapidly in ice-cold ACSF containing (in mM) 125 NaCl, 2.5 KCl, 1 MgCl<sub>2</sub>, 1.25 NaH<sub>2</sub>PO<sub>4</sub>, 2 CaCl<sub>2</sub>, 26 NaHCO<sub>3</sub>, 25 dextrose; osmolarity 315–325 mOsm, bubbled with 95% O<sub>2</sub>/5% CO<sub>2</sub>, pH 7.4. Visual cortex slices (300  $\mu$ m) were cut coronally (HM 650 V Vibration Microtome, MICROM) and incubated at 34 °C for 30 min before they were transferred to the recording chamber. Recording pipettes were filled with (in mM): 5 KCl, 115 potassium gluconate,

10 K-HEPES, 4 Mg-ATP, 0.3 Na-GTP, 10 sodium phosphocreatine; 40  $\mu$ M Alexa Fluor 594 and 0.1% biocytin (wt/vol); 290–295 mOsm, pH 7.2. The chloride reversal potential was  $\sim$ -85.2 mV. Liquid junction potential was not corrected for. Cells were approached under visual guidance using laser-scanning Dodt contrast imaging, and simultaneous two-photon imaging allowed detection of fluorescence from tdTomato-expressing cells. Whole-cell recordings were carried out in 32 °C ACSF, using Multiclamp 700b amplifiers (Axon Instruments) and custom software running on IGOR Pro (WaveMetrics Inc.). Step currents from -200/-100/-50 pA to 700/350/175 pA at 50/25/12.5 pA increments were injected to determine *I-V* relationship. Spike threshold was measured from the inflexion point of the minimally suprathreshold trace. Spike height was the difference between spike threshold and peak. Spike half-width was measured at the mean of threshold and peak. Cells were classified according to firing pattern<sup>1</sup> (**Supplementary Fig. 1a–e**). For accurate measurement of spike parameters, cells were included only if the series resistance was <30 M $\Omega$ .

***In vitro* mapping of connectivity between neurons functionally characterized *in vivo*.** Connectivity mapping experiments were performed both in C57Bl/6 mice (8 fast-spiking cells) and PV-Cre  $\times$  lsl-tdTomato transgenic mice (11 PV cells) as described<sup>11</sup>. Briefly, after *in vivo* two-photon calcium imaging of visual responses, small volumes of red fluorescent microspheres (Lumafuor) were injected into the imaged region to facilitate identification of the region in the coronally sliced brain. Whole-cell recordings from up to four cells simultaneously were carried out in the vicinity of the microsphere tract. The presence of synaptic connections was tested by evoking five spikes at 30 Hz in each cell, repeated 30–90 times. PPR was calculated as the amplitude of the second evoked EPSP over that of the first one. After connectivity mapping, step currents were injected to obtain *I-V* relationship. Cells were classified according to firing pattern and spike shape<sup>1</sup>. Out of 19 fast-spiking PV interneurons patched whose responses were characterized *in vivo* (of which 17 were significantly responsive to drifting gratings), 5 were classic non-accommodating, 5 were delayed classic non-accommodating, 4 were accommodating, and *I-V* curve was not obtained for 5 cells (lost after connectivity mapping). To match the same neurons imaged *in vivo* and recorded from *in vitro*, we performed three-dimensional image registration of *in vivo* and *in vitro* image stacks by affine transformation subsequent to the experiment. To relate connectivity to functional properties, we used the asymptotic Cochran-Armitage test for trend to test for significance.

48. Nimmerjahn, A., Kirchhoff, F., Kerr, J.N.D. & Helmchen, F. Sulforhodamine 101 as a specific marker of astroglia in the neocortex *in vivo*. *Nat. Methods* **1**, 31–37 (2004).

49. Brainard, D.H. The psychophysics toolbox. *Spat. Vis.* **10**, 433–436 (1997).

50. Tanahira, C. *et al.* Parvalbumin neurons in the forebrain as revealed by PV-Cre transgenic mice. *Neurosci. Res.* **63**, 213–223 (2009).